Disruption of *Cdh23* exon 68 splicing leads to progressive hearing loss in mice by affecting tip-link stability

Nana Li[a,1], Shuang Liu[b,1], Dange Zhao[c,1], Haibo Du[a], Yuehui Xi[a], Xiaoxi Wei[c], Qingling Liu[b], Ulrich Müller[d], Qing Lu[c,2], Wei Xiong[b,2], Zhigang Xu[a,e,2]

[a]Shandong Provincial Key Laboratory of Animal Cells and Developmental Biology and Key Laboratory for Experimental Teratology of the Ministry of Education, School of Life Sciences, Shandong University, Qingdao, Shandong 266237, China

[b]Chinese Institute for Brain Research, Beijing 102206, China

[c]Key Laboratory for the Genetics of Developmental and Neuropsychiatric Disorders, Ministry of Education, Bio-X Institutes, Shanghai Jiao Tong University, Shanghai 200030, China.

[d]The Solomon H. Snyder Department of Neuroscience, Johns Hopkins University School of Medicine, Baltimore, MD 21205, USA

[e]Shandong Provincial Collaborative Innovation Center of Cell Biology, Shandong Normal University, Jinan, Shandong 250014, China

[1]Contributed equally to this work

[2]Corresponding author: xuzg@sdu.edu.cn (Zhigang Xu); wei_xiong@cibr.ac.cn (Wei Xiong); luqing67@sjtu.edu.cn (Qing Lu)

Classification: Biological Sciences/Neuroscience

Keywords: CDH23; alternative splicing; hair cells; tip links; mechano-electrical transduction

Abstract

Inner ear hair cells are characterized by the F-actin-based stereocilia that are arranged into a staircase-like pattern on the apical surface of each hair cell. The tips of shorter-row stereocilia are connected with the shafts of their neighboring taller-row stereocilia through extracellular links named tip links, which are required for mechano-electrical transduction (MET) in hair cells. Cadherin 23 (CDH23) forms the upper part of tip links, and its cytoplasmic tail is inserted into the so-called upper tip-link density (UTLD) that contains other proteins such as harmonin. *Cdh23* gene contains 69 exons, and exon 68 is subjected to inner ear-specific alternative splicing. In the present work, we show that the *Cdh23(+68)* transcript is predominantly expressed in cochlear hair cells; however, deletion of *Cdh23* exon 68 does not affect tip link formation in mice. Further examination revealed that the stability of tip links is compromised by *Cdh23* exon 68 deletion, and *Cdh23* exon 68 knockout mice suffer from progressive and noise-induced hearing loss. Moreover, we show that the cytoplasmic tail of CDH23(+68) but not CDH23(-68) is engaged in phase separation-mediated condensate formation together with harmonin. In conclusion, our work suggests that alternative splicing of *Cdh23* exon 68 is necessary for the stability of tip links through regulating condensate formation of UTLD components.

Significance statement

Mechano-electrical transduction (MET) in inner ear hair cells requires tip links, which are formed by single-transmembrane proteins cadherin 23 (CDH23) and protocadherin 15 (PCDH15). The *Cdh23* gene is subjected to alternative splicing and exon 68 is only expressed in the inner ear. The physiological significance of this tissue-specific splicing of *Cdh23* exon 68 has remained elusive. Here we show that *Cdh23* exon 68 is necessary for maintaining tip-link stability, and mice with a *Cdh23* exon 68 deletion suffer from progressive and noise-induced hearing loss. We also provide evidence that exon 68 regulates CDH23 homodimerization and condensate formation with harmonin, a cytoplasmic binding partner for CDH23 that is concentrated at the tip-link insertion point near CDH23.

Introduction

As the mechanosensitive receptor cells in the inner ear, hair cells are characterized by their hair bundles on the apical cell surface. The hair bundle of each hair cell consists of one tubulin-based kinocilium and dozens of F-actin-based stereocilia (1). The kinocilium plays an important role in hair bundle development, but is not necessary for mechano-electrical transduction (MET) (2, 3). The kinocilium is lost in mature cochlear hair cells, whereas it persists in mature vestibular hair cells (1). On the other hand, the stereocilia are indispensable for MET, organized into rows of increasing height forming a staircase-like pattern in each hair cell (2). Various types of extracellular links provide connections between individual stereocilia as well as between the kinocilium and its neighboring tallest-row stereocilia in each hair cell. These linkages include tip links, horizontal top-connectors, lateral links, ankle links, and kinocilial links (4-6). Tip links connect the tips of shorter-row stereocilia with the shafts of neighboring taller-row stereocilia and are important for MET (4, 6, 7). When mechanical force deflects stereocilia towards the taller edge of the hair bundle, the tension in tip links is thought to increase, which in turn affects the open probability of MET channels localized near the lower end of tip links, resulting in the influx of cations into hair cells (2, 8, 9).

Two single-transmembrane cadherins, cadherin 23 (CDH23) and protocadherin 15 (PCDH15), have been shown to be essential components of lateral links, kinocilial links, and tip links (10-16). In tip links, CDH23 and PCDH15 form cis-homodimers through lateral interaction and trans-interact with each other via their N-terminal

extracellular cadherin (EC) domains, forming the upper and lower part of tip links, respectively (12) (Fig. 1A). Mutations of *CDH23* and *PCDH15* gene cause syndromic and non-syndromic hearing loss in human (17-20). Consistently, mutations in the *Cdh23* and *Pcdh15* gene in mice lead to deficits in the stereocilia and tip links, as well as to hearing loss (21-23). The upper and lower ends of tip links are anchored to the stereociliary membrane in electron-dense plaques referred to as upper tip-link density (UTLD) and lower tip-link density (LTLD), respectively (5, 24) (Fig. 1A). Immunolocalization studies revealed that UTLD components include Myosin VIIA (MYO7A), SANS, and harmonin in addition to the cytoplasmic tail of CDH23 (25, 26). Recently, it was suggested that MYO7A, SANS, and harmonin may form the UTLD via phase separation (27).

Transcription from different transcriptional start sites produces three main CDH23 isoforms, namely CDH23-V1 and CDH23-V2 with 27 and 7 extracellular EC domains, respectively, and CDH23-V3, which is a cytosolic protein (13) (Fig. 1B). Moreover, the *Cdh23* gene contains 69 exons, and exon 68 is subjected to alternative splicing thus gives rise to two CDH23 isoforms, CDH23(+68) and CDH23(-68) (10, 13, 28) (Fig. 1B). *Cdh23* is expressed in multiple tissues, whereas exon 68 inclusion has so far only been detected in the inner ear (29). Exon 68 is 105 base pairs (bp) long, encoding a peptide of 35 amino acids in the cytoplasmic tail of CDH23, which regulates the interaction of CDH23 with harmonin (28). Immunoreactivity with an antibody against this exon 68-encoded peptide specifically localizes to the stereocilia, raising the possibility that CDH23(+68) might be the CDH23 isoform that forms tip

links (10). However, the physiological significance of *Cdh23* exon 68 alternative splicing is unknown.

To explore the biological role of exon 68 splicing, we established knockout mice with *Cdh23* exon 68 deleted. Unexpectedly, tip links still form and function in young knockout mice, suggesting that CDH23(+68) is not essential for tip link formation. However, knockout of exon 68 leads to loss of tip links and degeneration of shorter-row mechanosensory stereocilia in aged mice or mice exposed to noise, suggesting that CDH23(+68) is required for the stability of tip links. Further

hypothesis that CDH23(+68) is the main CDH23 isoform that forms tip links in cochlear hair cells.

We then employed injectoporation experiments to examine the localization of different CDH23 isoforms in cochlear hair cells. Expression vectors for different CDH23 isoforms with an HA tag at their C-termini were introduced into cochlear hair cells. Immunostaining with anti-HA antibody revealed that for the longest CDH23 isoform (V1), both CDH23(+68) and CDH23(-68) were localized to the stereocilia as well as in the cell body (Fig. 1E). For the second longest isoform (V2), both CDH23(+68) and CDH23(-68) were only detected in the cell body (Fig. 1E). Similar cytoplasmic localization was observed for the shortest isoform (V3) (Fig. 1E). As mentioned above, different from V1 and V2 isoforms that contain transmembrane segments, CDH23-V3 is a short, cytosolic protein, and adding a tag to its C terminus might affect its subcellular localization. Therefore, we added the HA tag to the N terminus of CDH23-V3, which was detected in the stereocilia as well as cell body in injectoporated hair cells (Fig. 1E). Together, our present data demonstrate that V1 and V3 isoforms of CDH23 can localize to the stereocilia.

Deletion of *Cdh23* exon 68 leads to hearing loss but not balance deficits. To investigate the function of *Cdh23* exon 68 splicing, we established knockout mice with *Cdh23* exon 68 deleted using the clustered regularly interspaced short palindromic repeat (CRISPR)/CRISPR-associated protein 9 (Cas9) genome editing technique (Fig. 2A). Sanger sequencing confirmed that a deletion of 218 bp including

the entire exon 68 was introduced into the genome of the knockout mice (Fig. S1A and B). The obtained F0 mouse was in a C57BL/6 and CBA/CaJ mixed background, which was then crossed back to CBA/CaJ wild-type mice to generate heterozygous and eventually homozygous knockout mice. C57BL/6 but not CBA/CaJ mice carry the hypomorphic *Cdh23*^{753A} allele that causes progressive hearing loss (30). Sanger sequencing revealed that the heterozygous and homozygous knockout mice only carried the *Cdh23*^{753G} allele (Fig. S1C), therefore excluding the potential interference of the *Cdh23*^{753A} site on our following analysis.

RT-PCR results confirmed that *Cdh23(+68)* was no longer expressed in the cochlea of the knockout mice (Fig. 2B). Auditory b

RT-PCR results also confirmed that *Cdh23(+68)* was no longer expressed in the vestibule of knockout mice (Fig. S3A). We evaluated the vestibular function of *Cdh23* $^{68\gamma\ 68}$ mice by performing rotarod test, swimming test, tail hanging test, stereotyped circling movement test, retropulsion test, and head bobbing test. *Cdh23*$^{v2J/v2J}$ mice were included as positive control, which have been shown to possess balance deficits (22). *Cdh23*$^{v2J/v2J}$ mice indeed showed severe balance deficits, whereas vestibular function of *Cdh23* $^{68\gamma\ 68}$ mice was not significantly different from *Cdh23*$^{+\gamma\ 68}$ mice when examined at age of 7 months (Fig. 2F - K). Consistently, phalloidin staining and scanning electron microscopy (SEM) suggested that hair bundle morphology in vestibular hair cells was unaffected in 7-month-old *Cdh23* $^{68\gamma\ 68}$ mice (Fig. S3B - D'). Taken together, our data suggest that *Cdh23* $^{68\gamma\ 68}$ mice have hearing loss but preserved vestibular function.

Deletion of *Cdh23* exon 68 does not affect tip link formation or MET function in young mice. CDH23 has been shown to be a component of tip links, lateral links, and kinocilial links in developing hair cells (10, 13-16). In mature cochlear hair cells, however, CDH23 is mainly present in tip links, as lateral links and kinocilial links are transient structures that only exist in developing cochlear hair cells (6, 10, 12). We therefore examined tip links in mature cochlear hair cells of *Cdh23* exon 68 knockout mice, initially by analyzing the expression of CDH23 using immunohistochemistry with a custom antibody that detects the CDH23(+68) and CDH23 (-68) cytoplasmic tail. CDH23 was detected near the tip of stereocilia in control mice but not

Cdh23$^{v2J/v2J}$ mice at P8, confirming the specificity of the antibody and the absence of tip links in *Cdh23*$^{v2J/v2J}$ mice (Fig. 3A and B). Stereociliary tip localization of CDH23 was also observed in P8 *Cdh23* $^{68\Delta 68}$ mice, suggesting that tip link formation was unaffected by *Cdh23* exon 68 deletion (Fig. 3A and B). Next, we carried out SEM analysis to examine the shape of stereociliary tips. Beveled tips are thought to result from tip-link-mediated tension and are therefore a proxy for the presence of tip links (5, 7, 24, 31). We focused on the second-row stereocilia, whose relatively large dimension facilitates measurement of tip shape. Beveled second-row stereociliary tips were detected in the cochlear hair cells from P8 *Cdh23* $^{68\Delta 68}$ and control mice, but not in *Cdh23*$^{v2J/v2J}$ mice, suggesting that tip link formation was not affected by *Cdh23* exon 68 deletion (Fig. 3C and D). Lastly, we directly quantified the numbers of tip links in SEM images. Tip link numbers were comparable in control mice and *Cdh23* $^{68\Delta 68}$ mutants (Fig. 3E and F).

Normal tip link formation suggests that MET function might be preserved in young *Cdh23* $^{68\Delta 68}$ mice. To test this hypothesis, FM1-43FX dye uptake experiments were performed in mice of different genotypes. Up to P30, FM1-43FX dye uptake in *Cdh23* $^{68\Delta 68}$ hair cells was indistinguishable to that in control *Cdh23*$^{+\Delta 68}$ hair cells (Fig. 3G and H). We then recorded and quantified maximal MET currents by patch clamping hair cells whose hair bundles were deflected with fluid-jet. An averaged peak MET current of 697 39 pA was recorded from P6-P8 *Cdh23* $^{68\Delta 68}$ OHCs, which is comparable to the current from control *Cdh23*$^{+\Delta 68}$ OHCs (701 21 pA) (Fig. 4A and B). We also analyzed MET current kinetics from P6-P8 OHCs in response to

10-ms bundle deflections ranging from -300 to 1000 nm using a stiff probe (Fig. 4C). The activation and adaptation time constant of MET currents was not significantly different between *Cdh23* $^{68/68}$ and control *Cdh23*$^{+/+}$ ^{68} mice (Fig. 4C - F). Lastly, we measured voltage-gated currents of OHCs, which again did not show any significant difference between *Cdh23* $^{68/68}$ and control *Cdh23*$^{+/+}$ ^{68} mice (Fig. 4G and H). We conclude that MET function of cochlear hair cells was unaffected in young *Cdh23* $^{68/68}$ mice.

Deletion of *Cdh23* exon 68 causes stereocilia degeneration and OHC loss in adult mice. ABR measurements revealed progressive hearing threshold elevation in *Cdh23* $^{68/68}$ mice (Fig. 2C). We then employed SEM to examine hair bundle morphology in *Cdh23* $^{68/68}$ mice at older ages. At one month of age, the morphology of hair bundles in *Cdh23* $^{68/68}$ mice appeared largely normal (Fig. 5A). However, significant hair bundle loss was detected in 5-month-old *Cdh23* $^{68/68}$ OHCs, especially in the basal cochlear turn, which was further exaggerated in 8-month-old *Cdh23* $^{68/68}$ OHCs (Fig. 5A and B). High-magnification SEM showed that degeneration of third-row stereocilia was detected in *Cdh23* $^{68/68}$ OHCs at as early as P14, with increasing degeneration at subsequent ages (Fig. 5C and D). Degeneration of third-row stereocilia was also observed in inner hair cells (IHCs) of *Cdh23* $^{68/68}$ mice at P14 (Fig. 6A and B), albeit no complete hair bundle loss was detected in *Cdh23* $^{68/68}$ IHCs up to 8 months (Fig. 5A).

Immunostaining with an antibody against the hair cell marker MYO7A revealed

significant OHC loss in the basal cochlear turn of 5-month-old *Cdh23* $^{68/\ 68}$ mice (Fig. S4A, B, and D). By 8 months of age, OHC loss becomes more severe and extends to the apical cochlear turn in *Cdh23* $^{68/\ 68}$ mice (Fig. S4C and D). Meanwhile, no significant IHC loss was detected in *Cdh23* $^{68/\ 68}$ mice at any time points examined (Fig. S4A-C). Taken together, our data show that deletion of *Cdh23* exon 68 leads to stereocilia degeneration and OHC loss in adult mice.

Adult *Cdh23* $^{68/\ 68}$ mice show decreased tip-link numbers and compromised MET. Degeneration of third-row mechanosensitive stereocilia might result from loss of tip links in adult *Cdh23* $^{68/\ 68}$ mice. High-magnification SEM was then employed to examine beveled stereociliary tips and tip-link numbers in adult mice. Beveled second-row stereociliary tips were less prominent in 5-month-old *Cdh23* $^{68/\ 68}$ IHCs (Fig. 6C), and tip-link numbers were significantly reduced in 8-month-old *Cdh23* $^{68/\ 68}$ OHCs and IHCs (Fig. 6D and E). Furthermore, the intensity of CDH23 immunoreactivity was decreased in 5-month-old *Cdh23* $^{68/\ 68}$ OHCs (Fig. 6F and G). Finally, FM1-43FX uptake was also decreased in 5-month-old *Cdh23* $^{68/\ 68}$ cochlear hair cells (Fig. 6H and I). Taken together, our data suggest that *Cdh23* exon 68 deletion affects the stability of tip links thus leading to tip-link loss as mice age, which in turn is expected to compromise MET and lead to hearing loss.

Deletion of *Cdh23* exon 68 contributes to noise-induced hearing loss. Tip-link stability is affected by noise exposure that causes hearing loss (32, 33). We wanted to

determine whether adult *Cdh23* $^{68J/J}$ mice were more vulnerable to acoustic trauma. Exposure to a broadband noise of 2-20 kHz at 96 dB sound pressure level (SPL) for 2 hours caused a temporary threshold shift (TTS) in *Cdh23*$^{+/+}$ mice, with normal ABR thresholds restored 14 days later (Fig. 7A and B). The same noise exposure paradigm led to greater, permanent threshold shift (PTS) in *Cdh23* $^{68J/J}$ mice (Fig. 7A and B). Consistently, SEM revealed that noise exposure induces enhanced OHC hair bundle loss in *Cdh23* $^{68J/J}$ mice at both 1 day and 14 days after noise exposure (Fig. 7C and D). High-magnification SEM further revealed significant degeneration of third-row stereocilia in *Cdh23* $^{68J/J}$ OHCs (Fig. 7E and F) and IHCs 14 days after exposure to noise (Fig. 8A and B).

To our surprise, high-magnification SEM revealed that beveled second-row stereociliary tips in *Cdh23* $^{68J/J}$ IHCs, similar to control *Cdh23*$^{+/+}$ mice, were still present after noise exposure (Fig. 8C). Similarly, direct examination of tip links using SEM did not reveal a significant difference in tip-link numbers between *Cdh23* $^{68J/J}$ and control *Cdh23*$^{+/+}$ mice after noise exposure (Fig. 8D and E). Strikingly, CDH23 immunoreactivity was significantly decreased in *Cdh23* $^{68J/J}$ mice at 1 day and 14 days after noise exposure (Fig. 8F and G). In addition, FM1-43FX uptake was also significantly decreased in *Cdh23* $^{68J/J}$ mice at 1 day and 14 days after noise exposure, suggesting of compromised MET function (Fig. 8H and I). Taken together, our data suggest that *Cdh23* $^{68J/J}$ mice are more vulnerable to acoustic trauma.

Exon 68 of CDH23 affects harmonin condensate formation. To gain insights into

the mechanisms by which *Cdh23* alternative splicing regulates tip-link stability, we carried out biochemical experiments. It has been suggested that the exon 68-encoded peptide induces dimerization of the cytoplasmic tail of CDH23 (34). Consistently, yeast two-hybrid and co-immunoprecipitation (co-IP) results showed that the cytoplasmic tail of CDH23(+68) but not CDH23(-68) mediates homo-dimerization (Fig. 9A and B). Furthermore, co-sedimentation assays confirmed that the purified cytoplasmic tail of CDH23(+68) was more enriched in the pellet fraction than the cytoplasmic tail of CDH23(-68) (Fig. 9C).

The cytoplasmic tail of CDH23 interacts with harmonin, which has been suggested to participate in UTLD formation via phase separation together with MYO7A and SANS (27, 28, 35-37). We therefore determined whether *Cdh23* exon 68 splicing affects condensate formation of CDH23 and harmonin. The longest harmonin isoform (harmonin-b) contains a N-terminal domain (NTD), three PDZ domains, two coiled-coil (CC) domains, and a proline, serine, and threonine-rich (PST) domain. Harmonin binds to the cytoplasmic tail of CDH23 through its NTD and the second PDZ domain (PDZ2) (25, 28, 35, 36). Therefore, we performed co-sedimentation assays with the purified CDH23 cytoplasmic tail and harmonin NPDZ12 fragment that contains the NTD and the first two PDZ domains. CDH23(+68) predominantly co-sedimented with the harmonin NPDZ12 fragment (Fig. 9D). When the Cy3-labeled CDH23(+68) cytoplasmic tail was mixed with Alexa 488-labeled harmonin NPDZ12 fragment, significant spherical droplets with enrichment of both proteins were observed by fluorescence microscopy (Fig. 9E). Moreover, these droplets formed in a

dose-dependent manner (Fig. 9F). In contrast, the CDH23(-68) cytoplasmic tail barely formed large droplets with the harmonin NPDZ12 fragment (Fig. 9E and 9F). We then conducted fluorescence recovery after photobleaching (FRAP) assay to evaluate the mobility of CDH23(+68) cytoplasmic tail within the droplets. Within eight minutes after photobleaching, only 20-40% of the fluorescence signal recovered (Fig. 9G and 9H), suggesting that CDH23(+68) cytoplasmic tail forms solid-like condensates with harmonin. Taken together, our results provide evidence that exon 68 of CDH23 plays a role in the assembly of condensates involving harmonin.

Discussion

About the alternative splicing of *Cdh23* exon 68, two intriguing questions have remained unanswered for many years. First, how is this inner ear-specific splicing regulated? Second, what is the biological significance of this alternative splicing? Our recent work provided the answer to the first question. Through cell-based screening, we found that alternative splicing of *Cdh23* exon 68 is promoted by RBM24 and RBM38, and inhibited by PTBP1 (38). Moreover, the inclusion of *Cdh23* exon 68 is almost completely abolished in the cochlea of *Rbm24* knockout mice (39). Our present work now provides insights into the answer to the second question. Our data suggest that *Cdh23* exon 68 is important for maintaining the stability of tip links through regulating UTLD formation.

Our RT-PCR results showed that *Cdh23(+68)* transcript is predominantly expressed in postnatal cochlear hair cells, implying that CDH23(+68) but not CDH23(-68) is the

main CDH23 isoform that forms tip links in mature hair cells. Surprisingly, the formation and function of tip links are largely unaffected in young mice with *Cdh23* exon 68 deleted. Several lines of evidence support this conclusion. First, CDH23 immunoreactivity in the stereocilia is unaffected in young *Cdh23* $^{68/+68}$ mice. Second, beveled stereociliary tips, an indicator of the presence of functional tip links, is unaffected in young *Cdh23* $^{68/+68}$ mice. Third, tip links directly examined using SEM is unaffected in young *Cdh23* $^{68/+68}$ mice. Fourth, *Cdh23* exon 68 deletion in young mice does not affect FM1-43FX dye uptake, an indicator of functional integrity of hair cells. Last, the electrophysiology results confirmed that *Cdh23* exon 68 deletion does not affect MET in young mice. Together, our present data reveal that albeit CDH23(+68) mainly forms tip links in native hair cells, CDH23(-68) could fulfill this function when CDH23(+68) is absent.

However, the CDH23(-68)-mediated tip links are less stable than regular CDH23(+68)-mediated tip links. It has been shown that tip links are sensitive to environmental insults such as aging and noise (23, 32, 40). Our data reveal that the number of tip links is significantly decreased in aged *Cdh23* $^{68/+68}$ mice. Moreover, aged *Cdh23* $^{68/+68}$ mice show robust stereocilia degeneration and reduced FM1-43FX dye uptake. Consistently, *Cdh23* $^{68/+68}$ mice manifest progressive hearing loss. Therefore, our present data suggest that deletion of *Cdh23* exon 68 affects the stability of tip links, and eventually contributes to progressive hearing loss. Inclusion of *Cdh23* exon 68 happens in both the cochlea and vestibula. However, in contrast to auditory system, no balance deficits could be detected in *Cdh23* $^{68/+68}$ mice up to 7 months of

age. Compared to cochlear stereocilia, vestibular stereocilia are subjected to less intense daily stimuli, which might explain why tip links in vestibular hair cells are more stable even when exon 68 is absent.

When subjected to noise stimuli that lead to TTS in control mice, *Cdh23* $^{68/\Delta 68}$ mice manifest PTS with greater threshold elevation. Enhanced stereocilia degeneration and reduced FM1-43FX dye uptake were also observed in noise-exposed *Cdh23* $^{68/\Delta 68}$ mice. However, the number of tip links was unaffected when examined 1 day or 14 days after noise exposure. It has been suggested that tip links recover within seconds to hours after disruption by Ca^{2+} chelation (41-43). It's tempting to speculate that tip-link recovery might also happen quickly in a similar time scale after noise exposure, which explains why we did not detect tip-link loss in noise-exposed mice. Nevertheless, the temporary tip-link loss might lead to stereocilia degeneration, which could not be restored easily and eventually contribute to the observed noise-induced hearing loss. Consistent with this hypothesis, loss of tip links could only be detected in adult *Cdh23* $^{68/\Delta 68}$ mice at rather late age.

Further investigation showed that the CDH23(+68) cytoplasmic tail is more prone to dimerize and form condensates than the CDH23(-68) cytoplasmic tail. It has been shown that the cytoplasmic tail of CDH23, as well as harmonin, MYO7A, and SANS interact with each other and form a so-called UTLD protein complex at the upper insertion site of tip links (5, 24-26). In line with this, harmonin, MYO7A, and SANS form condensates via phase separation (27). Moreover, the CDH23(+68) cytoplasmic tail and harmonin form large protein assemblies through multivalent interactions (34).

Our present data confirm that the cytoplasmic tail of CDH23(+68) but not CDH23(-68) dimerize and form condensates together with harmonin, suggesting that the CDH23(+68) cytoplasmic tail might contribute to the formation of the UTLD. Our data also imply that the CDH23 short isoform (CDH23-V3) might play an important role in this process. CDH23-V3(+68) can bind to CDH23-V1(+68), and therefore might contribute to the formation of a large protein condensate near the upper end of tip links through multivalent interactions with other UTLD components (Fig. S5).

Hearing threshold elevation was observed as early as P18 in *Cdh23* $^{68/-68}$ mice, by which time stereocilia morphology was largely normal, and MET function revealed by FM1-43FX uptake was also not significantly affected. Therefore, cochlear function that does not involve tip links and even stereocilia might be compromised by *Cdh23* exon 68 deletion. It has been shown that ribbon synapse numbers are significantly reduced in aged C57BL/6N mice that carry the hypomorphic *Cdh23*^{753A} allele, and repair of this mutation partially rescues the phenotype (44, 45). Further investigations are warranted to fully understand the potential role of CDH23 in the synapse.

Our injectoporation results revealed that CDH23 V1 and V3 but not V2 isoforms are localized to the stereocilia. The underlying mechanism of this differential transport of CDH23 isoforms is not fully understood. The lower tip-link component, PCDH15, has three different isoforms, namely PCDH15-CD1, -CD2, and -CD3, which share common extracellular and transmembrane domains but differ in the cytoplasmic tail (11). We and other groups have shown that Golgi-associated chaperon protein PIST as well as unconventional myosins MYO3A, MYO3B, and

MYO7A might play important roles in the differential transport of PCDH15 isoforms in a heterologous expression system (46, 47). Interestingly, we found that PIST also binds to the cytoplasmic PDZ-binding-interface (PBI) of CDH23 and regulates its membrane localization in a heterologous expression system (48). However, considering that all CDH23 isoforms share similar cytoplasmic tails, it seems unlikely that PIST or unconventional myosins differentially regulate the transport of CDH23 isoforms. Alternatively, CDH23's targeting to and/or retention in the stereocilia might require interaction of the N-terminal EC domains of CDH23 with the N-terminal PCDH15 EC domains (49). Therefore, it is tempting to speculate that CDH23-V2 was not present in stereocilia because it lacks PCDH15-binding sites present in CDH23-V1. Another possibility is that CDH23-V2 lacks a N-terminal signal peptide and is therefore unable to target to the plasma membrane. CDH23-V3, as a small soluble protein, might be transported to the steoreocilia through binding to the cytoplasmic tail of CDH23-V1.

Materials and Methods

Animal models, hair cell isolation and RT-PCR, injectoporation, whole-mount immunostaining, ABR measurement, DPOAE measurement, vestibular function examination, FM1-43FX uptake experiment, SEM, electrophysiology, noise exposure, yeast two-hybrid, co-IP and western blot, protein purification and co-sedimentation assay, protein labeling and fluorescent imaging, FRAP analysis, and statistical analysis are described in *SI Appendix, SI Materials and Methods*.

Data availability. All study data are included in the article and/or *SI Appendix*.

Acknowledgements. We thank Sen Wang, Xiaomin Zhao, and Haiyan Yu from the core facilities for life and environmental sciences, Shandong University for technical support in SEM and confocal microscopy. This work was supported by grants from National Key Research & Developmental Program of China (2022YFE0131900), National Natural Science Foundation of China (82192861, 82071051), China Ministry of Science and Technology (2021ZD0203304), and Shandong Provincial Natural Science Foundation (ZR2020ZD39).

Author contributions. Z.X. conceived and designed research; N.L., S.L., D.Z., H.D., Y.X., X.W., and Q.Liu performed research; N.L., S.L., U.M., Q.Lu, W.X., and Z.X. analyzed data; and N.L., U.M., Q.Lu, W.X., and Z.X. wrote the manuscript with contributions from all authors.

Competing interests. The authors declare no competing interests.

References

1. K. Kikuchi, D. Hilding, The development of the organ of Corti in the mouse. *Acta Otolaryngol.* **60**, 207-222 (1965).
2. A. J. Hudspeth, R. Jacobs, Stereocilia mediate transduction in vertebrate hair cells (auditory system/cilium/vestibular system). *Proc. Natl. Acad. Sci. U.S.A.* **76**, 1506-1509 (1979).
3. C. Jones *et al.*, Ciliary proteins link basal body polarization to planar cell polarity regulation. *Nat. Genet.* **40**, 69-77 (2008).
4. J. O. Pickles, S. D. Comis, M. P. Osborne, Cross-links between stereocilia in the guinea pig organ of Corti, and their possible relation to sensory transduction. *Hear. Res.* **15**, 103-112 (1984).
5. D. N. Furness, C. M. Hackney, Cross-links between stereocilia in the guinea-pig cochlea. *Hear. Res.* **18**, 177-188 (1985).
6. R. J. Goodyear, W. Marcotti, C. J. Kros, G. P. Richardson, Development and properties of stereociliary link types in hair cells of the mouse cochlea. *J. Comp. Neurol.* **485**, 75-85 (2005).
7. J. A. Assad, G. M. Shepherd, D. P. Corey, Tip-link integrity and mechanical transduction in vertebrate hair cells. *Neuron* **7**, 985-994 (1991).
8. M. Beurg, R. Fettiplace, J. H. Nam, A. J. Ricci, Localization of inner hair cell mechanotransducer channels using high-speed calcium imaging. *Nat. Neurosci.* **12**, 553-558 (2009).
9. X. Qiu, U. Müller, Sensing sound: Cellular specializations and molecular force

sensors. *Neuron* **110**, 3667-3687 (2022).

10. J. Siemens *et al.,* Cadherin 23 is a component of the tip link in hair-cell stereocilia. *Nature* **428**, 950-955 (2004).

11. Z. M. Ahmed *et al.*, The tip-link antigen, a protein associated with the transduction complex of sensory hair cells, is protocadherin-15. *J. Neurosci.* **26**, 7022-7034 (2006).

12. P. Kazmierczak *et al.,* Cadherin 23 and protocadherin 15 interact to form tip-link filaments in sensory hair cells. *Nature* **449**, 87-91 (2007).

13. A. Lagziel *et al.*, Spatiotemporal pattern and isoforms of cadherin 23 in wild type and waltzer mice during inner ear hair cell development. *Dev. Biol.* **280**, 295-306 (2005).

14. V. Michel *et al.*, Cadherin 23 is a component of the transient lateral links in the developing hair bundles of cochlear sensory cells. *Dev. Biol.* **280**, 281-294 (2005).

15. A. K. Rzadzinska, A. Derr, B. Kachar, K. Noben-Trauth, Sustained cadherin 23 expression in young and adult cochlea of normal and hearing-impaired mice. *Hear. Res.* **208**, 114-121 (2005).

16. R. J. Goodyear, A. Forge, P. K. Legan, G. P. Richardson, Asymmetric distribution of cadherin 23 and protocadherin 15 in the kinocilial links of avian sensory hair cells. *J. Comp. Neurol.* **518**, 4288-4297 (2010).

17. H. Bolz *et al.*, Mutation of CDH23, encoding a new member of the cadherin gene family, causes Usher syndrome type 1D. *Nat. Genet.* **27**, 108-112 (2001).

18. J. M. Bork *et al.*, Usher syndrome 1D and nonsyndromic autosomal recessive deafness DFNB12 are caused by allelic mutations of the novel cadherin-like gene CDH23. *Am. J. Hum. Genet.* **68**, 26-37 (2001).

19. Z. M. Ahmed *et al.*, Mutations of the protocadherin gene PCDH15 cause Usher syndrome type 1F. *Am. J. Hum. Genet.* **69**, 25-34 (2001).

20. K. N. Alagramam *et al.*, Mutations in the novel protocadherin PCDH15 cause Usher syndrome type 1F. *Hum. Mol. Genet.* **10**, 1709-1718 (2001).

21. K. N. Alagramam *et al.*, The mouse Ames waltzer hearing-loss mutant is caused by mutation of Pcdh15, a novel protocadherin gene. *Nat. Genet.* **27**, 99-102 (2001).

22. F. Di Palma *et al.*, Mutations in Cdh23, encoding a new type of cadherin, cause stereocilia disorganization in waltzer, the mouse model for Usher syndrome type 1D. *Nat. Genet.* **27**, 103-107 (2001).

23. M. Schwander *et al.*, A mouse model for nonsyndromic deafness (DFNB12) links hearing loss to defects in tip links of mechanosensory hair cells. *Proc. Natl. Acad. Sci. U.S.A.* **106**, 5252-5257 (2009).

24. B. Kachar, M. Parakkal, M. Kurc, Y. Zhao, P. G. Gillespie, High-resolution structure of hair-cell tip links. *Proc. Natl. Acad. Sci. U.S.A.* **97**, 13336-13341 (2000).

25. N. Grillet *et al.*, Harmonin mutations cause mechanotransduction defects in cochlear hair cells. *Neuron* **62**, 375-387 (2009).

26. M. Grati, B. Kachar, Myosin VIIa and sans localization at stereocilia upper

tip-link density implicates these Usher syndrome proteins in mechanotransduction. *Proc. Natl. Acad. Sci. U.S.A.* **108**, 11476-11481 (2011).

27. Y. He, J. Li, M. Zhang, Myosin VII, USH1C, and ANKS4B or USH1G together form condensed molecular assembly via liquid-liquid phase separation. *Cell Rep.* **29**, 974-986 (2019).

28. J. Siemens *et al.*, The Usher syndrome proteins cadherin 23 and harmonin form a complex by means of PDZ-domain interactions. *Proc. Natl. Acad. Sci. U.S.A.* **99**, 14946-14951 (2002).

29. Z. Xu, A. W. Peng, K. Oshima, S. Heller, MAGI-1, a candidate stereociliary scaffolding protein, associates with the tip-link component Cadherin 23. *J. Neurosci.* **28**, 11269-11276 (2008).

30. K. Noben-Trauth, Q. Zheng, K. R. Johnson, Association of cadherin 23 with polygenic inheritance and genetic modification of sensorineural

investigation. *J. Laryngol. Otol.* **103**, 1125-1129 (1989).

34. L. Wu, L. Pan, C. Zhang, M. Zhang, Large protein assemblies formed by multivalent interactions between cadherin23 and harmonin suggest a stable anchorage structure at the tip link of stereocilia. *J. Biol. Chem.* **287**, 33460-33471 (2012).

35. B. Boeda *et al.*, Myosin VIIa, harmonin and cadherin 23, three Usher I gene products that cooperate to shape the sensory hair cell bundle. *EMBO J.* **21**, 6689-6699 (2002).

36. L. Pan, J. Yan, L. Wu, M. Zhang, Assembling stable hair cell tip link complex via multidentate interactions between harmonin and cadherin 23. *Proc. Natl. Acad. Sci. U.S.A.* **106**, 5575-5580 (2009).

37. A. Bahloul *et al.*, Cadherin-23, myosin VIIa and harmonin, encoded by Usher syndrome type I genes, form a ternary complex and interact with membrane phospholipids. *Hum. Mol. Genet.* **19**, 3557-3565 (2010).

38. N. Li, H. Du, R. Ren, Y. Wang, Z. Xu, Alternative splicing of Cdh23 exon 68

135, 135-145 (1999).

41. Y. Zhao, E. N. Yamoah, P. G. Gillespie, Regeneration of broken tip links and restoration of mechanical transduction in hair cells. *Proc. Natl. Acad. Sci. U.S.A.* **93**, 15469-15474 (1996).

42. A. A. Indzhykulian *et al.*, Molecular remodeling of tip links underlies mechanosensory regeneration in auditory hair cells. *PLoS Biol.* **11**, e1001583 (2013).

43. R. G. Alonso, M. Tobin, P. Martin, A. J. Hudspeth, Fast recovery of disrupted tip links induced by mechanical displacement of hair bundles. *Proc. Natl. Acad. Sci. U.S.A.* **117**, 30722-30727 (2020).

44. J. Mianne *et al.*, Correction of the auditory phenotype in C57BL/6N mice via CRISPR/Cas9-mediated homology directed repair. *Genome Med.* **8**, 16 (2016).

45. J. Jeng *et al.*, Pathophysiological changes in inner hair cell ribbon synapses in the ageing mammalian cochlea. *J. Physiol.* **598**, 4339-4355 (2020).

46. H. Nie *et al.*, Plasma membrane targeting of Protocadherin 15 is regulated by the Golgi-associated chaperone protein PIST. *Neural Plast.* **2016**, 8580675 (2016).

47. A. Ballesteros, M. Yadav, R. Cui, K. Kurima, B. Kachar, Selective binding and transport of protocadherin 15 isoforms by stereocilia unconventional myosins in a heterologous expression system. *Sci. Rep.* **12**, 13764 (2022).

48. Z. Xu, K. Oshima, S. Heller, PIST regulates the intracellular trafficking and plasma membrane expression of cadherin 23. *BMC Cell Biol.* **11**, 80 (2010).

49. M. Sotomayor, W. A. Weihofen, R. Gaudet, D. P. Corey, Structure of a force-conveying cadherin bond essential for inner-ear mechanotransduction. *Nature* **492**, 128-132 (2012).

Figure Legends

Fig. 1. CDH23 isoforms show different expression patterns in mouse cochlea. (A) Schematic drawing of hair cell stereocilia and tip links. (B) Schematic drawing of various CDH23 isoforms. (C) RT-PCR results showing expression of *Cdh23(+68)* and *Cdh23(-68)* transcripts in mouse cochlear sensory epithelium and spiral ganglion cells at different ages as indicated. *β-actin* was included as an internal control. (D) RT-PCR results showing expression of *Cdh23(+68)* and *Cdh23(-68)* transcripts in mouse cochlea and isolated cochlear hair cells at P0 and P15. *Sox2* was included as an internal control for supporting cells. (E) Injectoporation results showing the subcellular localization of CDH23 V1, V2, and V3 isoforms in cochlear hair cells. Shown are single confocal images taken from the middle cochlear turn. HA-tagged CDH23 isoforms were recognized with anti-HA antibody (green). Hair cells were labelled using an anti-MYO7A antibody (red). Stereocilia were visualized using TRITC-conjugated phalloidin (magenta). Scale bar, 10 μm.

Fig. 2. *Cdh23* $^{68\gamma\ 68}$ mice show hearing loss but no balance deficits. (A) Schematic drawing of the strategy for construction of *Cdh23* exon 68 knockout mice. Exons are indicated by numbered boxes. Deleted region is labelled in red. The positions of gRNA targets are indicated by arrows. (B) RT-PCR results showing expression of *Cdh23(+68)* and *Cdh23(-68)* transcripts in the cochlea from P5 wild-type (WT), *Cdh23*$^{+/\ 68}$, *Cdh23* $^{68\gamma\ 68}$, and *Cdh23*$^{v2J/v2J}$ mice. *β-actin* was included as an internal control. (C) ABR thresholds to click stimuli in *Cdh23*$^{+/\ 68}$ and *Cdh23* $^{68\gamma\ 68}$ mice of

different ages as indicated. (D) ABR thresholds to pure tone stimuli in P18 *Cdh23*$^{+/\ 68}$ and *Cdh23* $^{68J\ 68}$ mice. (E) DPOAE thresholds to pure tone stimuli in P30 *Cdh23*$^{+/\ 68}$ and *Cdh23* $^{68J\ 68}$ mice. (F) - (K) Vestibular function of 7-month-old *Cdh23*$^{+/\ 68}$ and *Cdh23* $^{68J\ 68}$ mice was evaluated by performing rotarod test (F), swimming test (G), tail hanging reflex (H), stereotyped circling movement (I), retropulsion (J), and head bobbing (K). *Cdh23*$^{v2J/v2J}$ mice were included as positive control. The number of animals for each group is indicated in the brackets or by the number of symbols. The statistic test was performed via two-way ANOVA with

Cdh23$^{+/+}$ and *Cdh23*$^{tg/tg}$ OHCs and IHCs was examined by SEM. *Cdh23*$^{v2J/v2J}$ mice were included as negative control. Shown are single images taken from the middle cochlear turn. (D) Percentage of second-row stereocilia with beveled tips in middle-turn OHCs and IHCs was calculated from the SEM results similar to (C). (E) Tip links of P8 *Cdh23*$^{+/+}$ and *Cdh23*$^{tg/tg}$ OHCs and IHCs were examined by SEM. *Cdh23*$^{v2J/v2J}$ mice were included as negative control. Shown are single images taken from the middle cochlear turn. Triangles indicate stereocilia with tip links; asterisks indicate stereocilia without tip links. (F) Percentage of second- and third-row stereocilia with tip links in middle-turn OHCs and IHCs was calculated from the SEM results similar to (E). (G) FM1-43FX uptake by *Cdh23*$^{+/+}$ and *Cdh23*$^{tg/tg}$ cochlear hair cells at different ages as indicated was examined using confocal microscope. Shown are single confocal images taken from the middle cochlear turn. (H) FM1-43FX uptake in middle-turn cochlear hair cells was quantified according to the results similar to (G). Scale bars, 5 μm in (A), 1 μm in (C) and (E), 200 nm in the insets of (E), and 10 μm in (G). The cell numbers for each group are indicated by the numbers of symbols (or 50 for panel H) from at least three animals. The statistic test was performed via one-way ANOVA with Dunnett's multiple comparisons test (for panel B, F, and OHCs in panel D), Kruskal-Wallis test with Dunn's multiple comparisons (for IHCs in panel D), or Two-way ANOVA with Šídák's multiple comparisons test (for panel H). ns, not significant; ****, $p<0.0001$.

Fig. 4. MET currents are unaffected in young *Cdh23*$^{tg/tg}$ mice. (A) Representative

MET currents induced by fluid jet were examined in OHCs from *Cdh23*^{68} and *Cdh23* ^{68} mice. A 40-Hz sinusoidal fluid jet was delivered to the hair bundle. (B) Averaged peak MET currents from similar data as shown in (A). (C) Representative MET currents induced by a stiff probe were examined in OHCs from *Cdh23*^{68} and *Cdh23* ^{68} mice. A set of 10 msec-hair bundle deflections were delivered ranging from -300 nm to 1000 nm at 100 nm steps. (D) Activation time constant ($\vartheta_{activation}$) in *Cdh23*^{68} OHCs (0.1261 msec) and *Cdh23* ^{68} OHCs (0.1308 msec). (E) Time constants of fast adaptation (ϑ_{fast}) in *Cdh23*^{68} OHCs (0.7614 msec) and *Cdh23* ^{68} OHCs (0.7868 msec). (F) Time constants of slow adaptation (ϑ_{slow}) in *Cdh23*^{68} OHCs (9.101 msec) and *Cdh23* ^{68} OHCs (13.22 msec). (G) Voltage-gated currents were recorded from *Cdh23*^{68} and *Cdh23* ^{68} OHCs. The membrane potential was altered from -150 mV to +110 mV at 20 mV steps. (H) I-V curves were drawn from data similar to panel (G). In all panels, data were collected from P6-P8 OHCs from at least three mice with *Cdh23*^{68} shown in black and *Cdh23* ^{68} shown in red. Cell number is indicated in the brackets. The statistic test was performed via student's two-tailed unpaired *t* test. ns, not significant.

Fig. 5. Stereocilia maintenance is affected in adult *Cdh23* ^{68} cochlear hair cells. (A) Hair bundle morphology from *Cdh23*$^{+}$ ^{68} and *Cdh23* ^{68} mice at different ages and cochlear positions as indicated was examined by SEM. (B) OHC hair bundle numbers along successive 20-IHC intervals was calculated according to the SEM results similar to (A). (C) High-magnification SEM images of middle-turn OHC hair

bundles from *Cdh23*$^{+/+}$ and *Cdh23*$^{tm1.1Kjn/tm1.1Kjn}$ mice at different ages as indicated. First-row stereocilia are indicated in red; second-row stereocilia are indicated in yellow; third-row stereocilia are indicated in blue. (D) Numbers of third-row stereocilia with normal height per OHC at middle cochlear turn was calculated according to the SEM results similar to (C). Scale bars, 20 μm in (A), 1 μm in (C). The sample numbers for each group are indicated by the numbers of symbols from at least three animals. The statistic test was performed via two-way ANOVA with Tukey's multiple comparisons test. ns, not significant; *, $p<0.05$; ***, $p<0.001$; ****, $p<0.0001$.

Fig. 6. Tip links and FM1-43FX uptake are affected in adult *Cdh23*$^{tm1.1Kjn/tm1.1Kjn}$ mice. (A) High-magnification SEM images of middle-turn IHC hair bundles from *Cdh23*$^{+/+}$ and *Cdh23*$^{tm1.1Kjn/tm1.1Kjn}$ mice at different ages as indicated. First-row stereocilia are indicated in red; second-row stereocilia are indicated in yellow; third-row stereocilia are indicated in blue. (B) Numbers of third-row stereocilia with normal height per IHC at middle cochlear turn was calculated according to the SEM results similar to (A). (C) Percentage of second-row stereocilia with beveled tips in middle-turn IHCs was calculated from the SEM results similar to (A). (D) Tip links of 8-month-old *Cdh23*$^{+/tm1.1Kjn}$ and *Cdh23*$^{tm1.1Kjn/tm1.1Kjn}$ OHCs and IHCs were examined by SEM. Shown are single images taken from the middle cochlear turn. Triangles indicate stereocilia with tip links; asterisks indicate stereocilia without tip links. (E) Percentage of second- and third-row stereocilia with tip links in middle-turn OHCs and IHCs was calculated

from the SEM results similar to (D). (F) Localization of CDH23 in the stereocilia of 5-month-old *Cdh23*$^{+/+}$ and *Cdh23*$^{68J/68J}$ mice was examined by performing whole-mount immunostaining using an antibody against the cytoplasmic tail of CDH23 (green). Stereociliary F-actin was visualized with TRITC-conjugated phalloidin (magenta). Shown are single confocal images taken from the middle cochlear turn. (G) Quantification of CDH23 immunoreactivity in middle-turn cochlear hair cells according to the whole-mount immunostaining results similar to (F). (H) FM1-43FX uptake by 5-month-old *Cdh23*$^{+/+}$ and *Cdh23*$^{68J/68J}$ cochlear hair cells was examined using confocal microscope. Shown are single images taken from the middle cochlear turn. (I) FM1-43FX uptake in middle-turn cochlear hair cells was quantified according to the results similar to (H). Scale bars, 1 μm in (A) and (D), 200 nm in the insets of (D), 5 μm in (F), and 10 μm in (H). The cell numbers for each group are indicated by the numbers of symbols from at least three animals. The statistic test was performed via two-way ANOVA with Tukey's multiple comparisons test (for panels B and C), Mann-Whitney test (for panel E), or student's *t* test (for panels G and I). ns, not significant; **, $p<0.01$; ****, $p<0.0001$.

Fig. 7. *Cdh23*$^{68J/68J}$ mice show increased acoustic vulnerability. (A - B) One-month-old *Cdh23*$^{+/+}$ and *Cdh23*$^{68J/68J}$ mice were exposed to a broadband noise of 2-20 kHz at 96 dB SPL for 2 h, and mice of the same genotypes and ages without noise exposure were included as control groups (Ctl). Hearing thresholds to pure tone or click stimuli 1 day (A) or 14 days (B) after noise treatment were analyzed

by performing ABR measurements. (C) Hair bundle morphology from *Cdh23*$^{+/+}$ ^{68} and *Cdh23* $^{68/+}$ ^{68} basal-turn hair cells at different time after noise exposure was examined by SEM. (D) OHC hair bundle numbers along successive 20-IHC intervals in the basal cochlear turn was calculated according to the SEM results similar to (C). (E) High-magnification SEM images of middle-turn OHC hair bundles from *Cdh23*$^{+/+}$ ^{68} and *Cdh23* $^{68/+}$ ^{68} mice at different time after noise exposure. First-row stereocilia are indicated in red; second-row stereocilia are indicated in yellow; third-row stereocilia are indicated in blue. (F) Numbers of third-row stereocilia with normal height per OHC in the middle cochlear turn was calculated according to the SEM results similar to (E). Scale bars, 20 μm in (C), 1 μm in (E). The sample numbers for each group are indicated by the numbers of symbols from at least three animals. The statistic test was performed via two-way ANOVA with Tukey's multiple comparisons test (for panel D, F and click measurements in panels A, B), or two-way ANOVA with Šídák's multiple comparisons test (for pure-tune measurements in panels A, B). ns, not significant; *, $p<0.05$; **, $p<0.01$; ***, $p<0.001$; ****, $p<0.0001$.

Fig. 8. Stereocilia maintenance and FM1-43FX uptake are affected in noise-exposed *Cdh23* $^{68/+}$ ^{68} mice. (A) High-magnification SEM images of middle-turn IHC hair bundles from *Cdh23*$^{+/+}$ ^{68} and *Cdh23* $^{68/+}$ ^{68} mice at different time after noise exposure. First-row stereocilia are indicated in red; second-row stereocilia are indicated in yellow; third-row stereocilia are indicated in blue. (B) Numbers of

third-row stereocilia with normal height per IHC in the middle cochlear turn was calculated according to the SEM results similar to (A). (C) Percentage of second-row stereocilia with beveled tips in middle-turn hair cells was calculated from the SEM results similar to (A). (D) Tip links of *Cdh23*$^{+/+}$ ^{68} and *Cdh23* $^{68/+}$ ^{68} OHCs and IHCs at 14 days after noise exposure were examined by SEM. Shown are single images taken from the middle cochlear turn. Triangles indicate stereocilia with tip links. (E) Percentage of second- and third-row stereocilia with tip links in middle-turn hair cells was calculated from the SEM results similar to (D). (F) Localization of CDH23 in the stereocilia of *Cdh23*$^{+/+}$ ^{68} and *Cdh23* $^{68/+}$ ^{68} mice at different time after noise exposure was examined by performing whole-mount immunostaining using an antibody against the cytoplasmic tail of CDH23 (green). Stereociliary F-actin was visualized with TRITC-conjugated phalloidin (magenta). Shown are single confocal images taken from the middle cochlear turn. (G) Quantification of CDH23 immunoreactivity in middle-turn hair bundles according to the whole-mount immunostaining results similar to (F). (H) FM1-43FX uptake by *Cdh23*$^{+/+}$ ^{68} and *Cdh23* $^{68/+}$ ^{68} cochlear hair cells at different time after noise exposure was examined using confocal microscope. Shown are single images taken from the middle cochlear turn. (I) FM1-43FX uptake in middle-turn hair cells was quantified according to the results similar to (H). Scale bars, 1 μm in (A) and (D), 200 nm in the insets of (D), 2.5 μm in (F), and 10 μm in (H). The cell numbers for each group are indicated by the numbers of symbols from at least three animals. The statistic test was performed via two-way ANOVA with Tukey's multiple comparisons test (for panels B, G and I), Mann-Whitney test (for

panel C), or Mann-Whitney test (for panel E). ns, not significant; ***, $p<0.001$; ****, $p<0.0001$.

Fig. 9. Exon 68 is important for CDH23 dimerization and condensate formation. (A) Interaction between CDH23 isoforms examined by performing yeast two-hybrid assay. Left: Transformation efficiency is examined on SD-Leu-Trp medium, and protein-protein interaction is examined on SD-Leu-Trp-His-Ade medium. Right: Quantification of protein-protein interaction according to results similar to left. Nubl and pPR3-N are included as positive and negative controls, respectively. (B) Interaction between CDH23 isoforms examined by co-IP. Expression vectors were transfected into HEK293T cells to express GFP- or MYC-tagged CDH23 isoforms, and cell lysates were subjected to immunoprecipitation. IP indicates antibody used for immunoprecipitation, and WB indicates antibody used for detection. (C) Co-sedimentation results of CDH23 cytoplasmic tail (50 μM) showing that CDH23(+68) cytoplasmic tail was much more enriched in the pellet than CDH23(-68) cytoplasmic tail. S indicates supernatant, and P indicates pellet. (D) Co-sedimentation results of CDH23(+68) cytoplasmic tail mixed with harmonin NPDZ12 fragment. Both proteins were enriched in the pellet and the pellet fraction of the mixture exceeds that of CDH23(+68) cytoplasmic tail alone. (E) Fluorescence images showing that CDH23(+68) cytoplasmic tail/harmonin NPDZ12 fragment forms larger droplets than CDH23(-68) cytoplasmic tail/harmonin NPDZ12 fragment. CDH23 cytoplasmic tail and harmonin NPDZ12 fragment were labeled with Cy3 and Alexa 488, respectively.

Labeled proteins were added at a ratio of 1%. CDH23 cytoplasmic tail: 180 μM, harmonin NPDZ12 fragment: 45 μM. (F) Fluorescence images showing that the phase separation capacity of CDH23 cytoplasmic tail/harmonin NPDZ12 fragment is concentration-dependent. The concentration ratio of CDH23 cytoplasmic tail: harmonin NPDZ12 fragment is 4:1, and proteins were labeled in the same way as in (E). (G) Images showing the recovery process of CDH23(+68) cytoplasmic tail

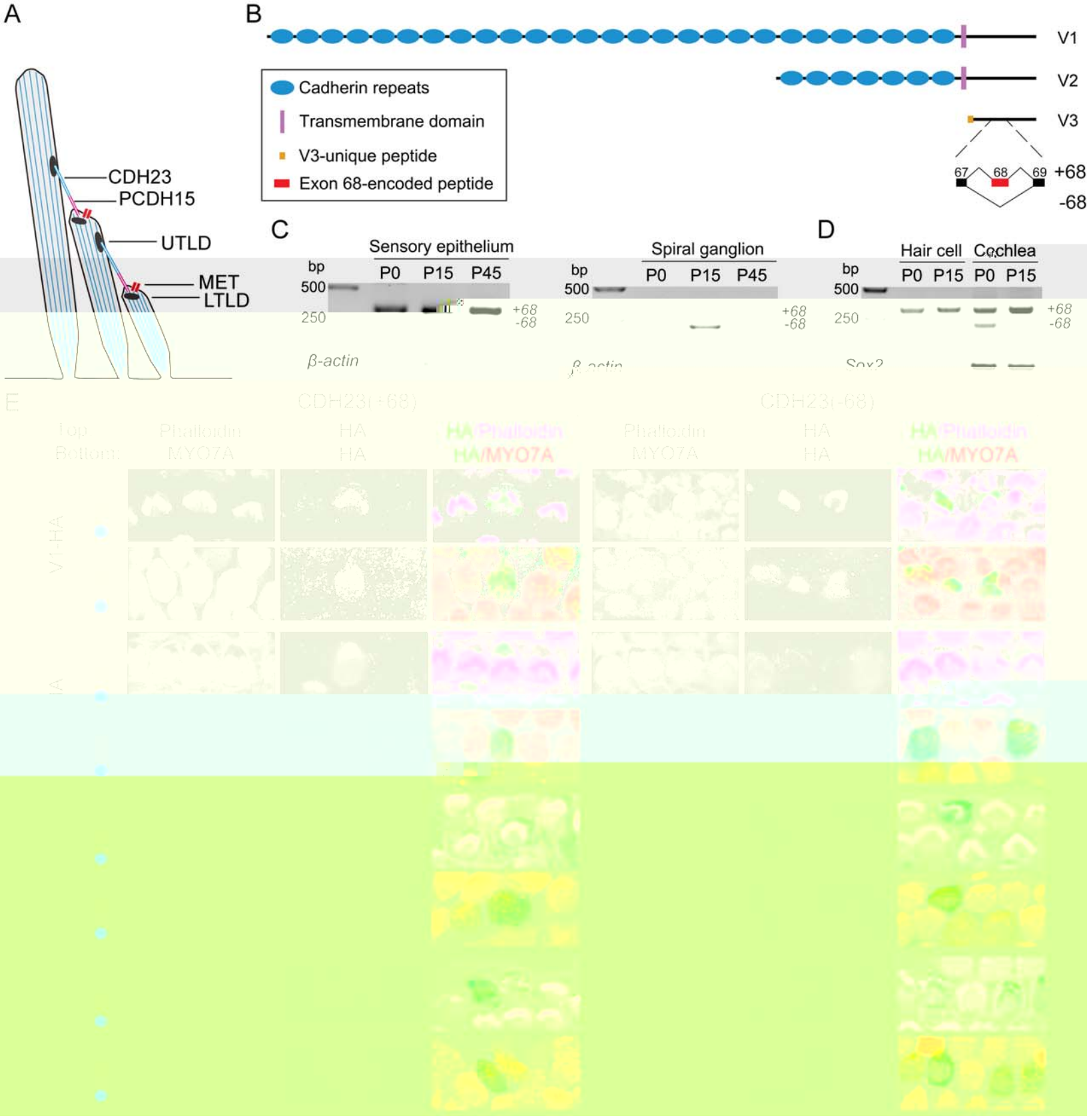
A
CDH23
PCDH15
UTLD
MET
LTLD
B
Cadherin repeats
Transmembrane domain
V3-unique peptide
Exon 68-encoded peptide
V1
V2
V3
67
68
69
+68
-68
C
Sensory epithelium
Spiral ganglion
bp
500
250
P0
P15
P45
+68
-68
β-actin
D
Hair cell
Cochlea
Sox2
E
CDH23(+68)
CDH23(-68)
Top
Bottom
Phalloidin
MYO7A
HA
HA/MYO7A
V1-HA

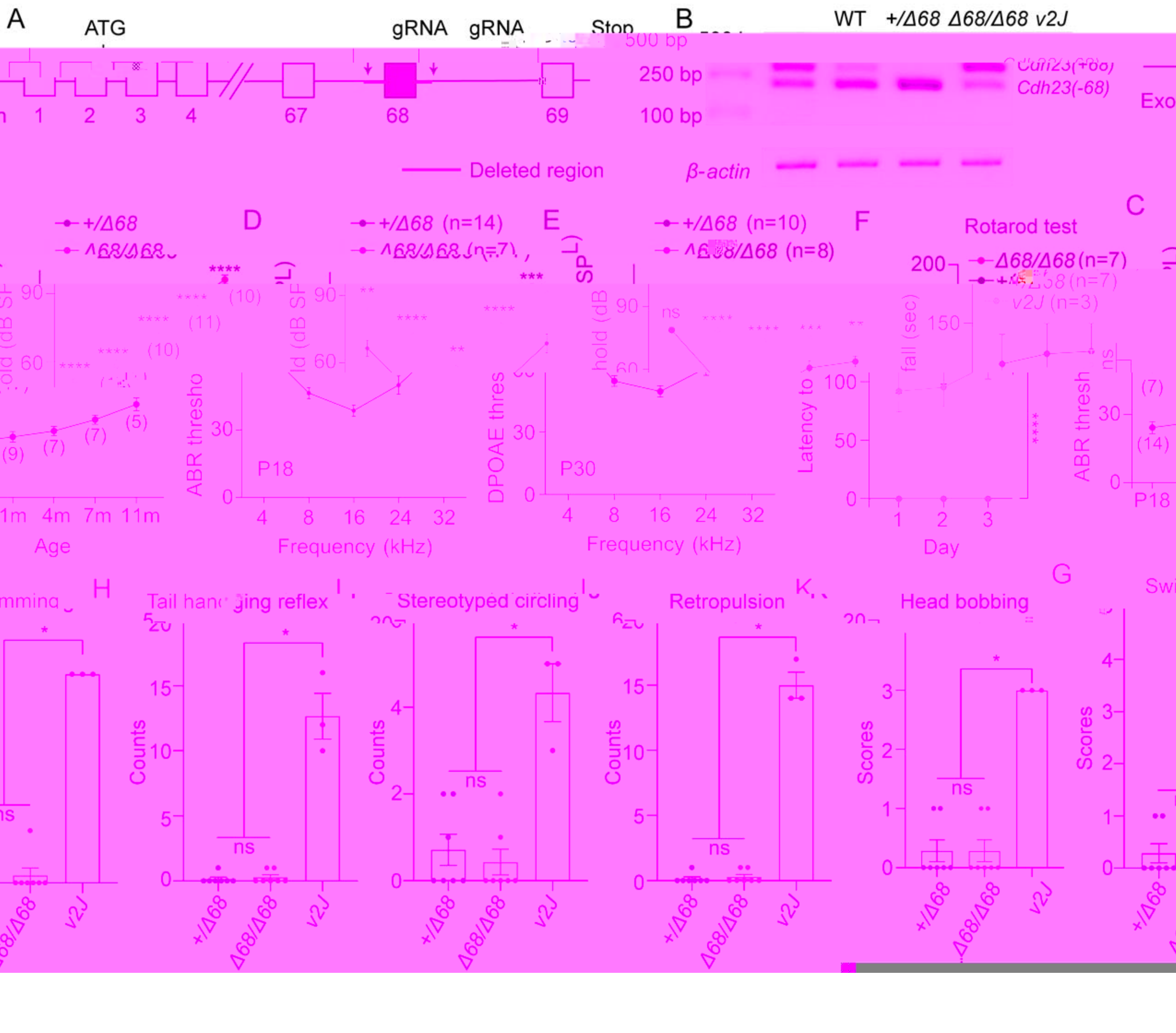
A
ATG
gRNA
gRNA
Stop
1
2
3
4
67
68
69
Deleted region
B
WT
+/Δ68
Δ68/Δ68
v2J
500 bp
250 bp
100 bp
Cdh23(+68)
Cdh23(-68)
β-actin
D
+/Δ68 (n=14)
P18
ABR threshold (dB SPL)
Frequency (kHz)
E
+/Δ68 (n=10)
Δ68/Δ68 (n=8)
P30
DPOAE threshold (dB SPL)
Frequency (kHz)
F
Rotarod test
Δ68/Δ68 (n=7)
+/Δ68 (n=7)
v2J (n=3)
Latency to fall (sec)
Day
Age
1m
4m
7m
11m
H
Tail hanging reflex
Counts
Stereotyped circling
Retropulsion
Head bobbing
Scores
+/Δ68
Δ68/Δ68
v2J
ns

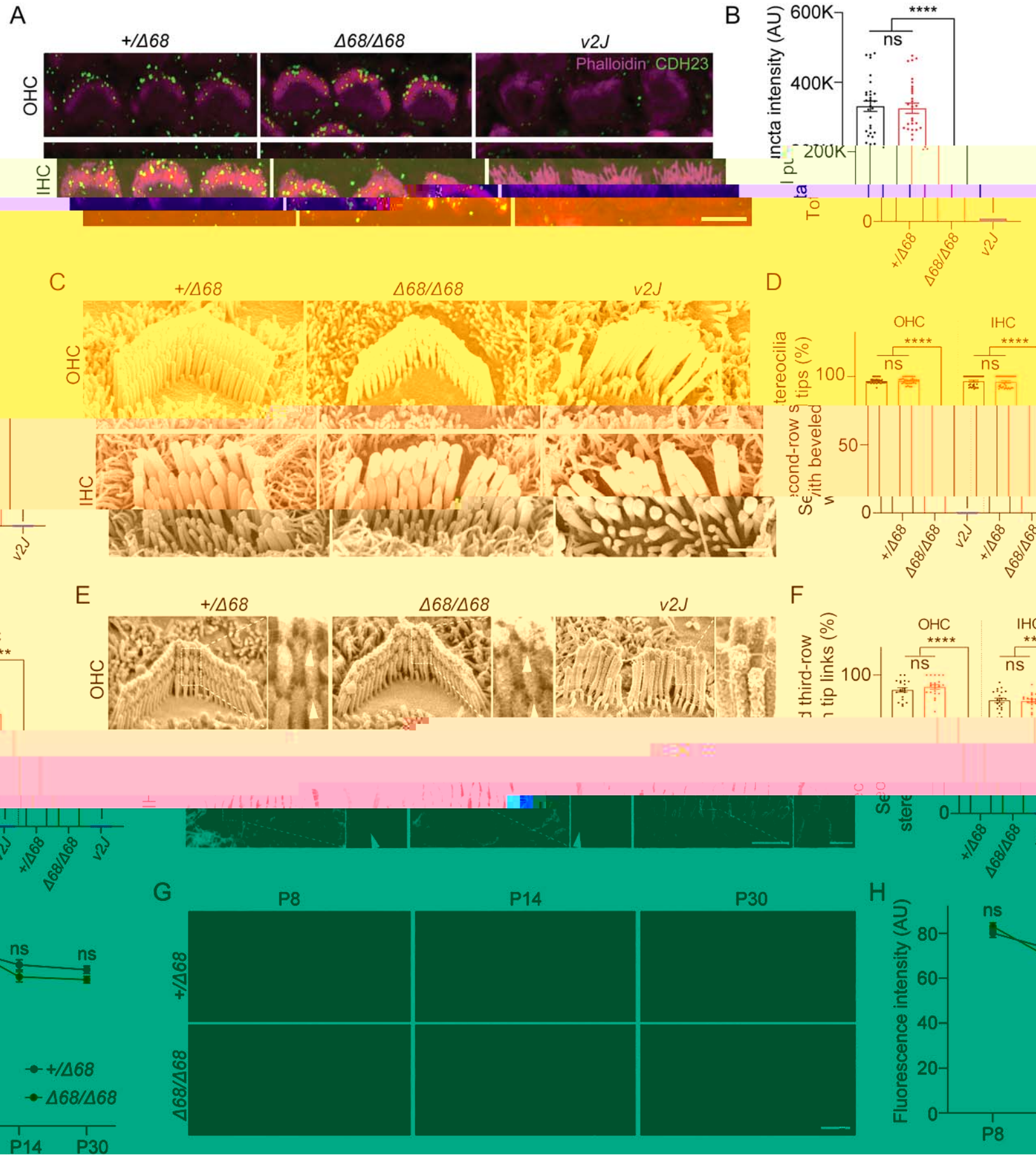
A
+/Δ68
Δ68/Δ68
v2J
OHC
IHC
Phalloidin CDH23
B
600K
400K
200K
0
****
ns
+/Δ68
Δ68/Δ68
v2J
C
+/Δ68
Δ68/Δ68
v2J
OHC
IHC
D
OHC
IHC
****
ns
100
50
0
+/Δ68
Δ68/Δ68
v2J
E
+/Δ68
Δ68/Δ68
v2J
OHC
F
OHC
IHC
****
ns
100
0
+/Δ68
Δ68/Δ68
ns
ns
+/Δ68
Δ68/Δ68
P14
P30
G
P8
P14
P30
+/Δ68
Δ68/Δ68
H
ns
80
60
40
20
0
P8

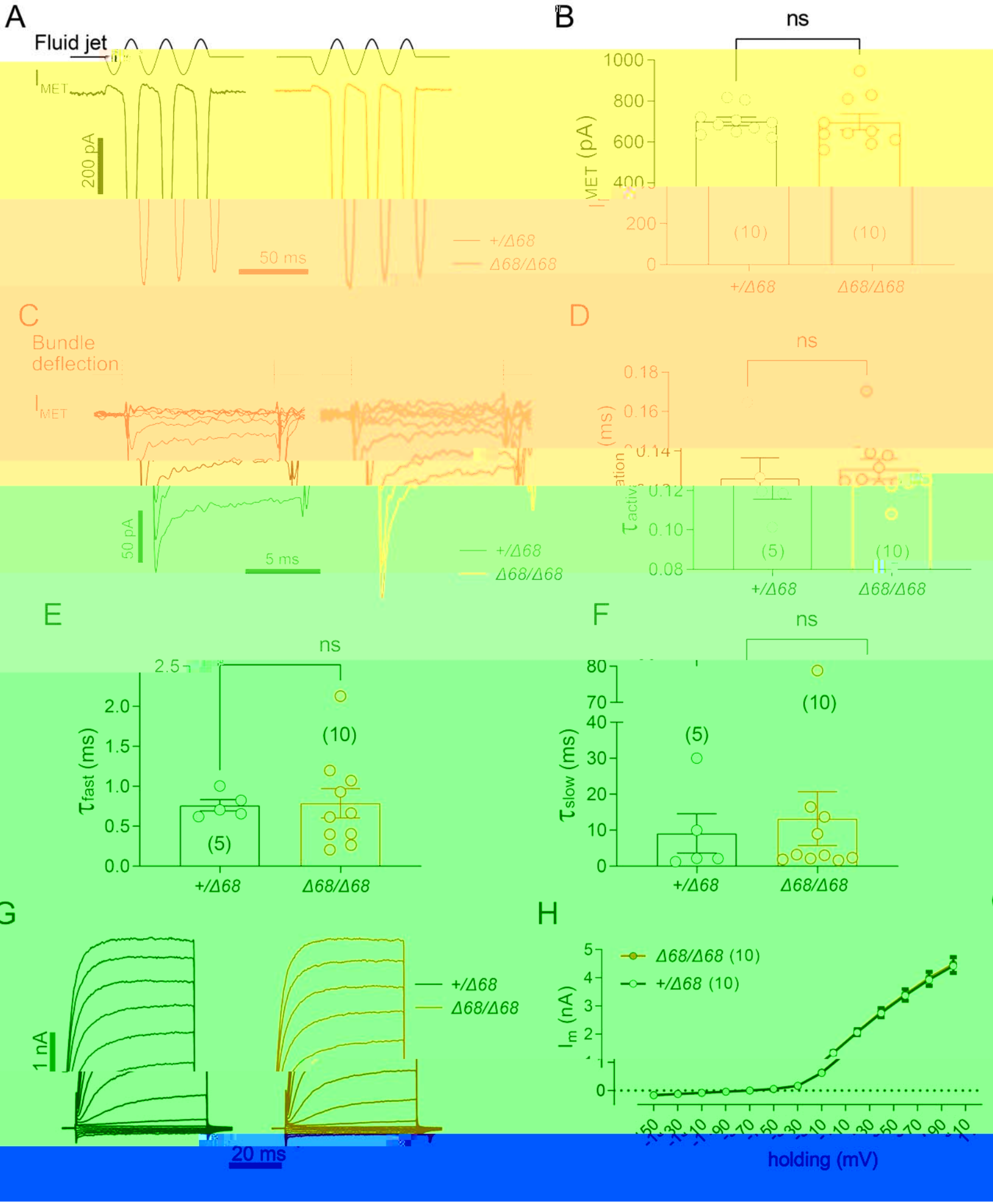
A
Fluid jet
I MET
200 pA
50 ms
+/Δ68
Δ68/Δ68
B
ns
I MET (pA)
1000
800
600
400
200
0
(10)
(10)
+/Δ68
Δ68/Δ68
C
Bundle deflection
I MET
50 pA
5 ms
+/Δ68
Δ68/Δ68
D
ns
(ms)
0.18
0.16
0.14
0.12
0.10
0.08
(5)
(10)
+/Δ68
Δ68/Δ68
E
ns
τfast (ms)
2.5
2.0
1.5
1.0
0.5
0.0
(5)
(10)
+/Δ68
Δ68/Δ68
F
ns
τslow (ms)
80
70
40
30
20
10
0
(5)
(10)
+/Δ68
Δ68/Δ68
G
1 nA
20 ms
+/Δ68
Δ68/Δ68
H
Δ68/Δ68 (10)
+/Δ68 (10)
Im (nA)
5
4
3
2
1
0
holding (mV)

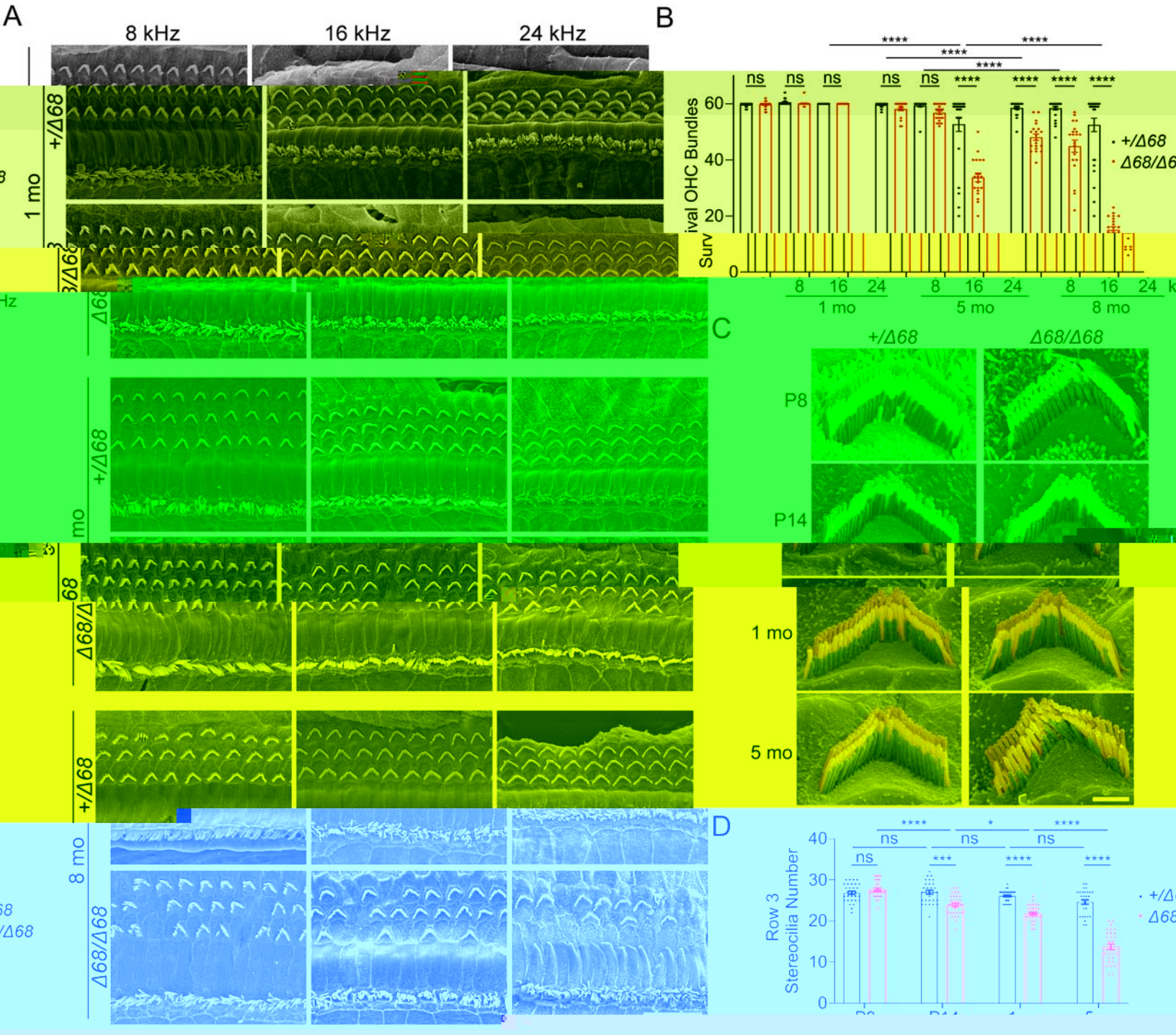
A
8 kHz
16 kHz
24 kHz
+/Δ68
1 mo
Δ68/Δ68
5 mo
8 mo
B
ival OHC Bundles
Surv
+/Δ68
Δ68/Δ6
ns
****
1 mo
5 mo
8 mo
C
+/Δ68
Δ68/Δ68
P8
P14
1 mo
5 mo
D
Row 3
Stereocilia Number
ns
***
****
*

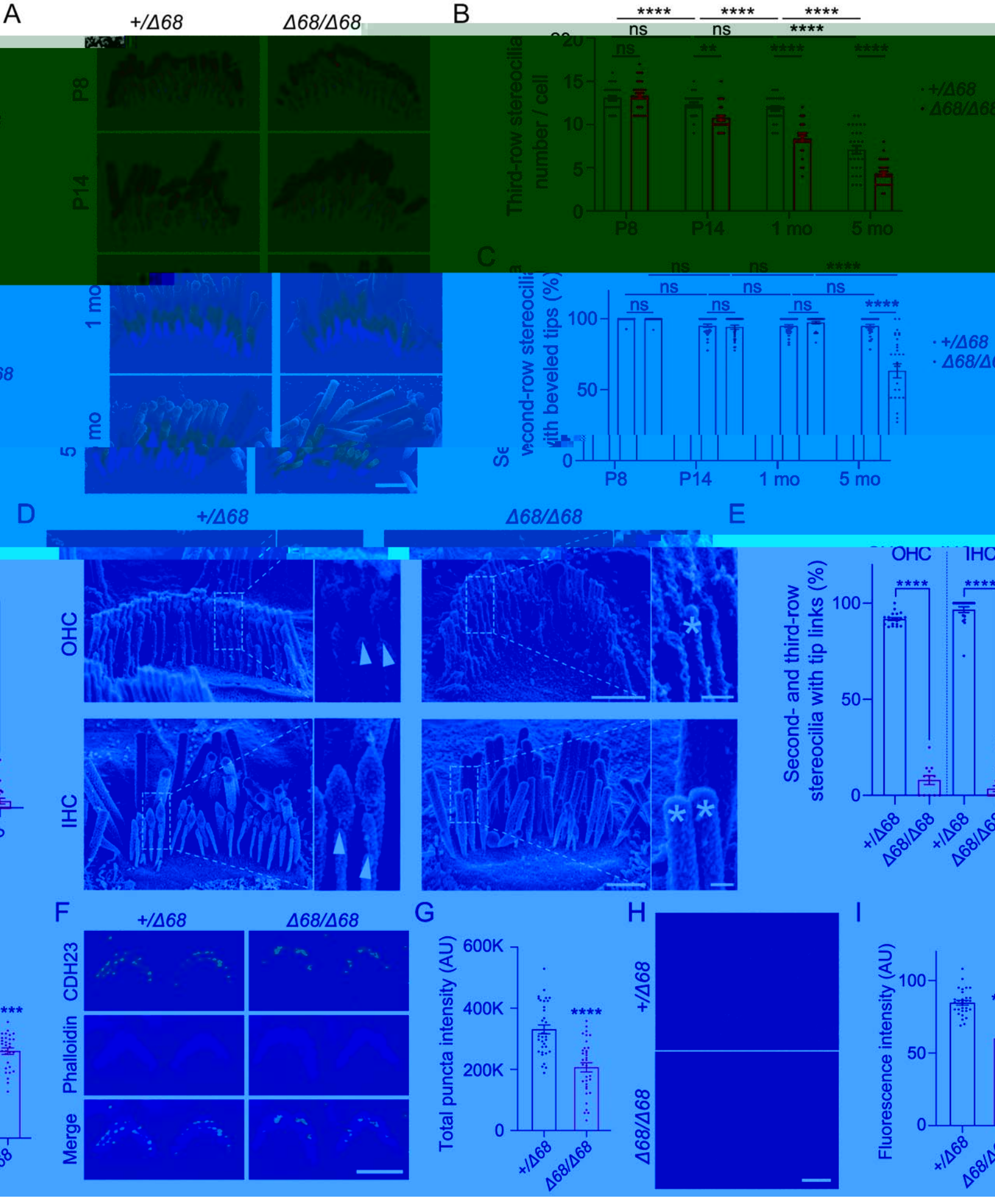
A
+/Δ68
Δ68/Δ68
P8
P14
1 mo
5 mo
B
Third-row stereocilia number / cell
P8
P14
1 mo
5 mo
ns
**
****
C
Second-row stereocilia with beveled tips (%)
D
OHC
IHC
E
Second- and third-row stereocilia with tip links (%)
F
CDH23
Phalloidin
Merge
G
Total puncta intensity (AU)
600K
400K
200K
0
H
I
Fluorescence intensity (AU)

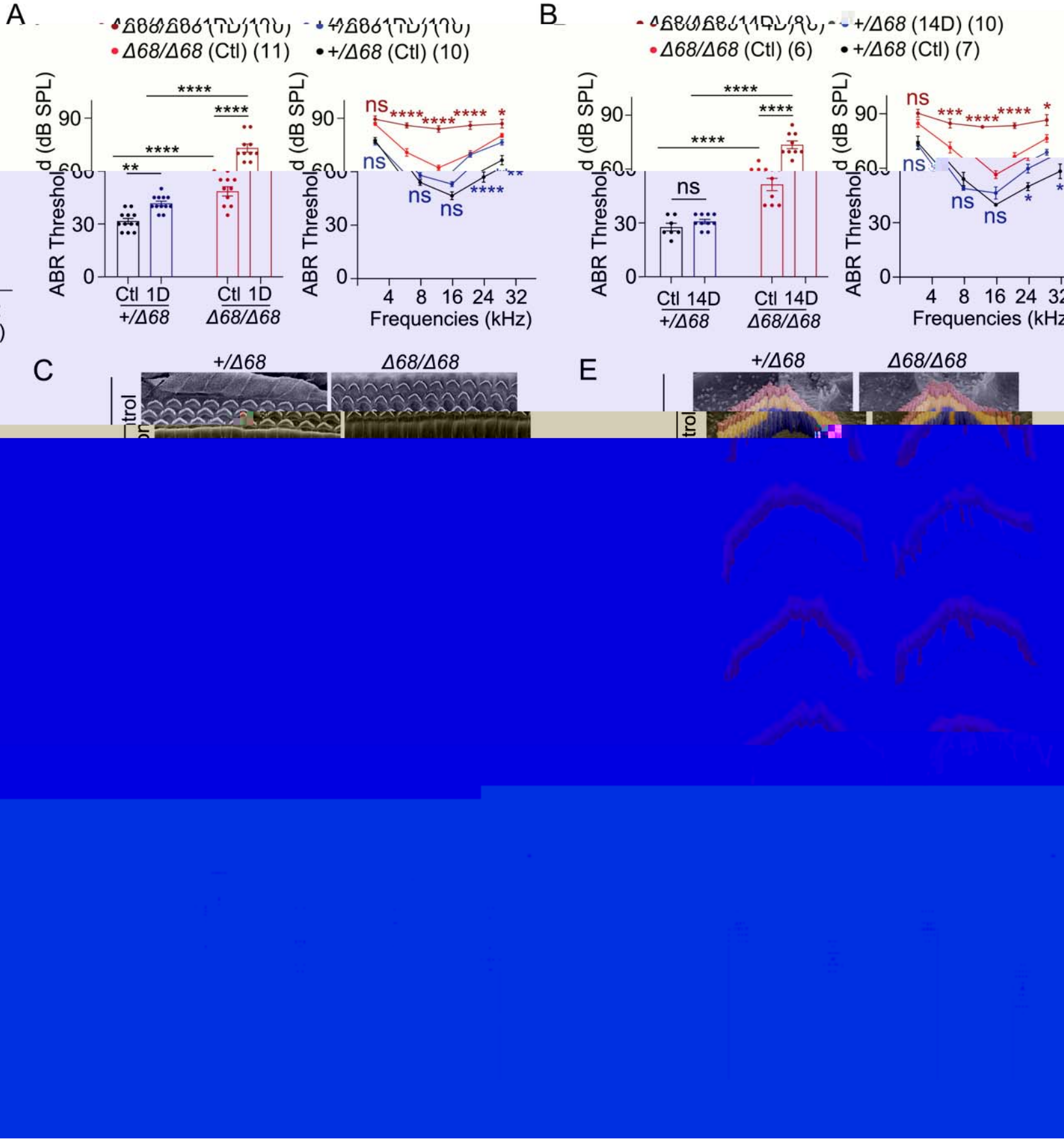
A
Δ68/Δ68 (Ctl) (11)
+/Δ68 (Ctl) (10)
ABR Threshold (dB SPL)
Ctl 1D
+/Δ68
Ctl 1D
Δ68/Δ68
Frequencies (kHz)
B
+/Δ68 (14D) (10)
Δ68/Δ68 (Ctl) (6)
+/Δ68 (Ctl) (7)
Ctl 14D
+/Δ68
Ctl 14D
Δ68/Δ68
C
+/Δ68
Δ68/Δ68
E
+/Δ68
Δ68/Δ68


A
+/Δ68
Δ68/Δ68
B
Control
C
CDH23
1D
14D
H
+/Δ68
Δ68/Δ68
I
150
0
ns
****
Total

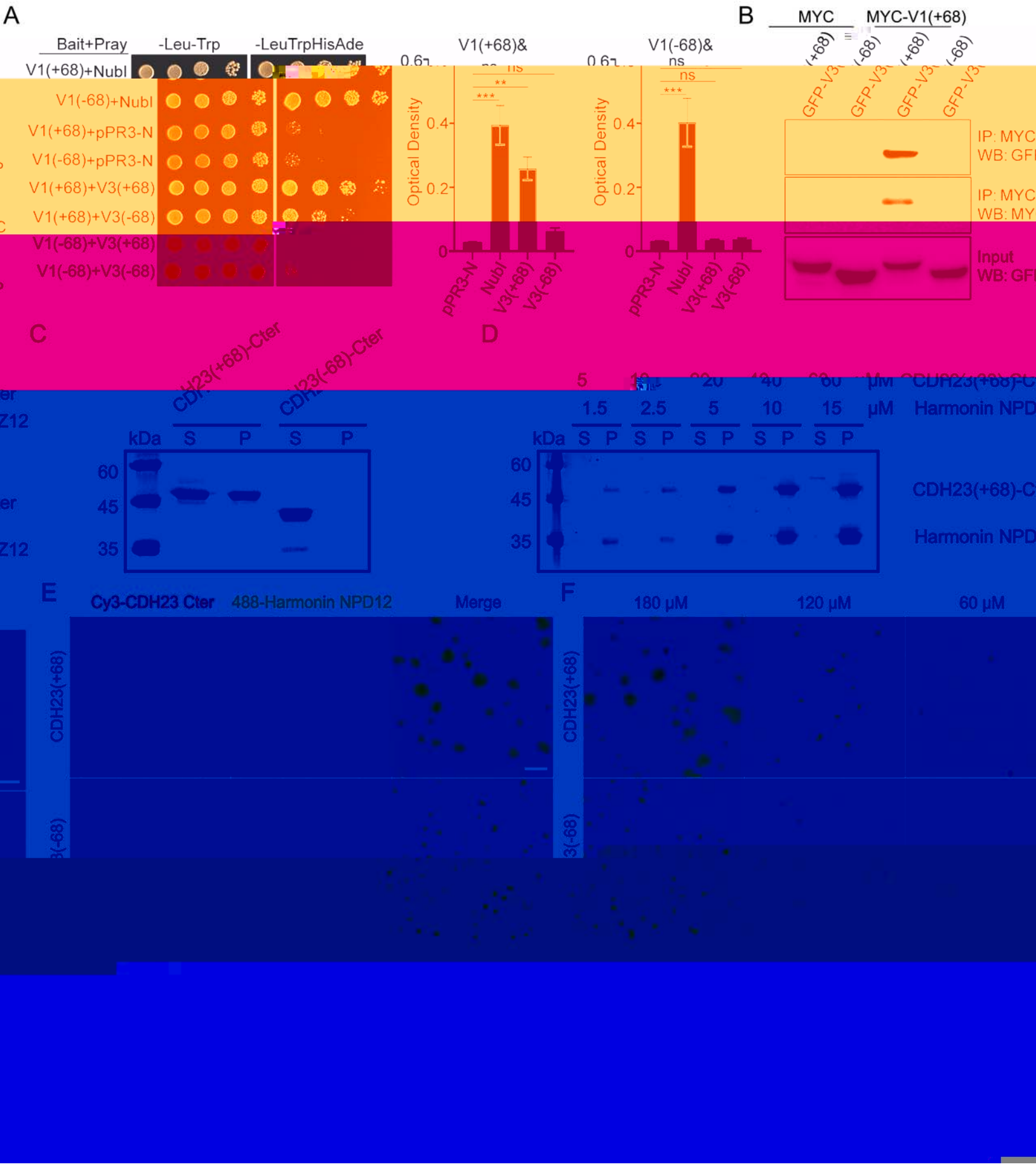
A
Bait+Pray
-Leu-Trp
-LeuTrpHisAde
V1(+68)+Nubl
V1(-68)+Nubl
V1(+68)+pPR3-N
V1(-68)+pPR3-N
V1(+68)+V3(+68)
V1(+68)+V3(-68)
V1(-68)+V3(+68)
V1(-68)+V3(-68)
V1(+68)&
V1(-68)&
Optical Density
0.6
0.4
0.2
0
ns
**
***
pPR3-N
Nubl
V3(+68)
V3(-68)
B
MYC
MYC-V1(+68)
GFP-V3(+68)
GFP-V3(-68)
IP: MYC
WB: GFP
IP: MYC
WB: MYC
Input
WB: GFP
C
CDH23(+68)-Cter
CDH23(-68)-Cter
kDa
S
P
60
45
35
D
μM
1.5
2.5
5
10
15
CDH23(+68)-C
Harmonin NPD
E
Cy3-CDH23 Cter
488-Harmonin NPD12
Merge
CDH23(+68)
F
180 μM
120 μM
60 μM